Energy xxx (2017) 1–8

Contents lists available at ScienceDirect

Energy

journal homepage: www.elsevier.com/locate/energy

# CFD analysis of roof tile coverings

Michele Bottarelli [a, *], Marco Bortoloni [b], Giovanni Zannoni [a], Richard Allen [c], Nigel Cherry [c]

[a] University of Ferrara, Via Quartieri 8, 44121 Ferrara, Italy
[b] University of Ferrara, Via Saragat 13, 44121 Ferrara, Italy
[c] Monier Technical Centre, Spectrum Hse, Beehive Ring Road, Crawley RH6 0LG, UK

ARTICLE INFO

*Article history:*
Received 14 August 2016
Received in revised form
10 March 2017
Accepted 16 March 2017
Available online xxx

*Keywords:*
Roof tiles
Above sheathing ventilation
Experimental air permeability
CFD
Novel tile shapes

ABSTRACT

In hot climates tiled pitched roofs significantly reduce the heat transfer across the roof structure, due to the ventilated air layer between tiles and roofing underlay formed by the arrangement of battens and counter-battens supporting the tiles. This so-called Above Sheathing Ventilation (ASV) depends on the air entering and leaving at the eaves, ridge and the gaps between the tiles. With a view towards higher energy savings in space cooling, the natural and forced convection occurring in ASV could be enhanced by increasing the roof air permeability by means of novel tile shapes, as here analysed in two stages.

The first stage of designing the new tile shapes was to measure the air permeability for a type of existing tile (Marseillaise style) using an experimental test rig, by monitoring the volumetric flow rate through the tiles over a range of pressure differences across the tiles. Then, a three-dimensional CFD model was implemented to replicate the full test rig geometry, and this was calibrated against the experimental data. In the next stage, the calibration was used to support the design of novel Marseillaise tile shapes, and to compare their performance against existing tiles. Finally, in order to analyse the variation in air flow under typical wind conditions for a pitched roof, a parametric study was undertaken, consisting of 72 scenarios varying wind speed, direction and angle of incidence.

An increase in volumetric flow rate through the tiles was found to be related not only to an increase in the open area between tiles, but also to the design of the tile locks. By redesigning the geometry of these locks, whilst still giving consideration to their primary purpose of preventing the ingress of driving rain, it was possible to yield an improvement in air permeability of up to 100% in comparison with the original designs. Additionally, these novel designs were shown to increase the air flow rate as the wind angle moved from being directly up the roof slope around to the side, in contrast to the decrease seen with existing tile shapes.



## 1. Introduction

Ventilated roofs can play an important role in reducing the energy requirement for space cooling and in increasing the indoor thermal comfort. In fact, the ventilated layer below the covering in ventilated roofs helps to dissipate the excess heat (due to solar radiation) by increasing the natural and forced air convection. This topic is relevant mainly in hot climates such as the Mediterranean regions, since the energy demand for air-conditioning in summer represents a significant financial and environmental cost.

In ventilated pitched roofs (Fig. 1), the arrangement of battens and counter-battens supporting the tiles forms a ventilation duct under the tiles so that air flows from the eaves to the ridge. In the case of discontinuous roof covering (e.g. roofing tiles), the ventilation is enhanced by the air permeability between the overlapping tiles, which provides an additional, distributed network of airflow paths in to and out of the ASV.

Several studies have demonstrated the performance of this so-called Above Sheathing Ventilation (ASV) in reducing solar heat gain. Laboratory tests were carried out in Ref. [1] to evaluate the airflow and the temperature distribution in ASV as a function of the solar radiation intensity and the geometry of the channel. Also full-scale models were prepared to run outdoor tests in Refs. [2] and [3]. The thermal performance of six different types of passive roof were

* Corresponding author.
*E-mail addresses:* michele.bottarelli@unife.it (M. Bottarelli), marco.bortoloni@unife.it (M. Bortoloni), giovanni.zannoni@unife.it (G. Zannoni), richard.allen@monier.com (R. Allen), nigel.cherry@monier.com (N. Cherry).

http://dx.doi.org/10.1016/j.energy.2017.03.081
0360-5442/

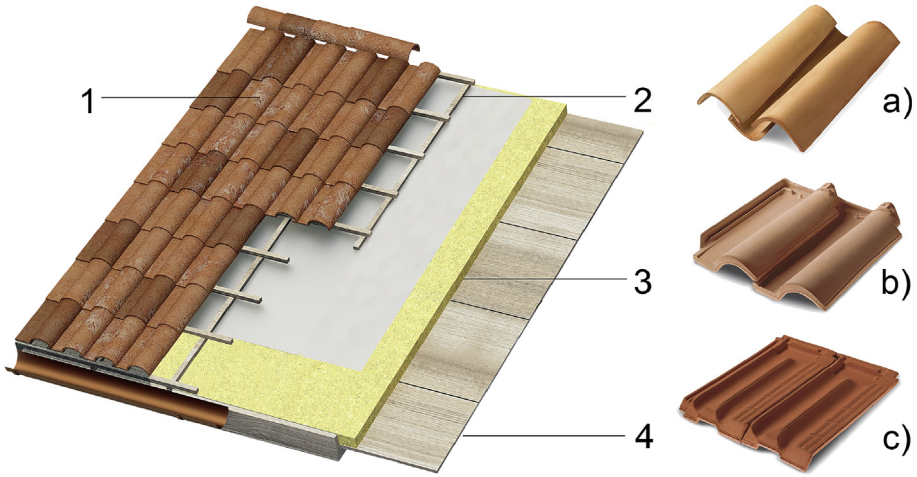


**Fig. 1.** Typical ventilated tiled pitched roof (1: roof tiles; 2: batten & counter-batten; 3: insulation; 4: deck), and most common types of roof tile (a: Coppo, b: Portuguese, c: Marseillaise).

monitored during very hot summer days in India, [4]. Among the different roofs, the ventilated pitched roof with a covering of clay tiles showed the optimum indoor thermal performance. The reduction of solar heat gain of a ventilated concrete tile was investigated in Ref. [5], in comparison with an ordinary corrugated roof tile. The thermal behaviour of a pitched roof with a covering in ceramic tiles and ventilated eaves was monitored by means of a scale model of a typical dwelling, observing a significant heat dissipation capacity [6]. A correlation between solar radiation and ventilation rate, based on experimental data, was discussed in Ref. [7]. Other works used numerical models to solve both air-flows and heat-transfer in ventilated roofs. A numerical approach was followed in Ref. [8] to quantify the thermal benefits of a tiled roof over a traditional shingle roof; the estimated benefit was about 14%. A numerical model was developed and validated against experimental data in Ref. [9], observing that the air flow induced by the buoyancy forces within the ventilated space reduces the heat flux into the attic by 30% compared to a direct-nailed roof. Similar results were obtained in Ref. [10] by means of a steady state numerical simulation of ventilated and microventilated roofs. The thermal behaviour of ventilated roofs was modelled with FLUENT in Ref. [11], showing that the heat fluxes can be reduced up to 50% during summer with ventilated roofs. Recently, a steady state numerical analysis was conducted by Ref. [12] simulating the natural convection due to buoyancy forces in ventilated roofs, as a function of solar radiation in different thermal conditions (summer and winter season).

But, whereas the majority of previous numerical studies neglected the tile air permeability modelling the ASV as an air duct, the effect of tile air permeability was numerically investigated in Ref. [13] using a 2D CFD model of a full building with simplified flat roof tiles, in which also the heat transfer was analysed. This work supported the idea that the air permeability of the roof tile coverings can increase the mass flow rate along the ventilation channel, thus improving the thermal performance of the roof during the summer season. According to [13], the air permeability of a discontinuous covering is a characteristic tied to a specific tile geometry and manufacturer, because it is intrinsically linked to the materials, manufacturing process and know-how of individual tile producer. In view of this, the ASV can be enhanced by improving the design of clay tiles with the aim of increasing the air permeability, as proposed in the European project LIFE HEROTILE (LIFE14CCA/IT/000939) for two basic shapes: Portuguese and Marseillaise type (Fig. 1b and c, traditional styles representative of the majority of the market in Southern Europe, described as “bold roll” and “low profile”, respectively).

In the present paper, the air permeability of clay roof tiles is experimentally and numerically analysed to compare a standard with novel tile shapes, which have been designed to improve the ASV in the preparatory action of the LIFE HEROTILE project. In addition, a parametric study is conducted to analyse the variation in the air flow passing through the tile for different wind intensity, directions and angle of incidence (Fig. 2). For the sake of brevity, only the analysis of some novel Marseillaise shapes are presented here in terms of methodology and results.

## 2. Methodology

The methodology combines experimental tests and numerical simulations to assess the roof tile air permeability and to predict the behaviour of novel tile shapes, designed to enhance the flow rate between laid tiles.

Preliminary tests at Monier Technical Centre (Heusenstamm, Germany) experimentally measured the air permeability of a covering built with an existing Marseillaise tile shape (type 2050, *SP* – standard production), using the pressure difference across the tiles at measured air flow rates. These results were used as the

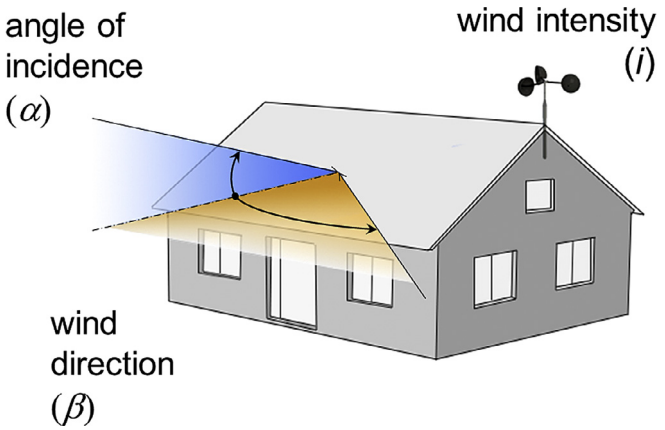


**Fig. 2.** Study parameterization.

Please cite this article in press as: Bottarelli M, et al., CFD analysis of roof tile coverings, Energy (2017), http://dx.doi.org/10.1016/j.energy.2017.03.081

benchmark to calibrate a CFD model replica of the test rig, in which the 3D model of the existing tiles (type 2050, *SM* – standard model) was implemented. Finally, the calibration was used as the basis for analysing the air permeability performance of a novel Marseillaise design (type 2032, *PM_00* – basic project model) and two evolutions (type 2032, *PM_02* and *PM_02n* – project model evolution 02 and 02n) with limited shape modifications, in comparison with the existing tile and the basic design. Fig. 3 shows the 3D model of the basic project *PM_00* showing the transversal section, which is compared against the *SM* standard model and the two evolutions *PM_02* and *PM_02n* in Fig. 4. The *PM_00* design is slightly bigger than *SM* and involves changes in the lower side of the tile and in both the headlock and sidelock geometry; in comparison with *PM_00*, the sidelock is higher in *PM_02* and *PM_02n*.

A similar methodology was previously applied in Ref. [14] to enhance the design of an existing Portuguese type, which has a different geometry with much higher roll compared with the Marseillaise type; in addition, in the present study, a parametric analysis of the wind behaviour was carried out. Four wind speeds ($i$ = 0.5, 1.0, 2.0, 5.0 m/s) were simulated blowing over the tiles, with three angles of incidence ($\alpha = 10°, 20°, 30°$) and six horizontal wind directions ($\beta$ = 0°, 15°, 30°, 45°, 60°, 80°), to represent a parametric analysis of 72 wind conditions over a common roof tile covering (Fig. 2).

### 2.1. Experimental rig

The experiment consisted of sucking (or blowing) air down a 100 mm pipe into a large wooden plenum (the "box", Fig. 5a), on top of which was an array of the tiles under investigation, compliant with the standard described in Ref. [15]. Constructed from 20 mm plywood, the box was designed to have a volume much larger than the volume flow rate through the tiles, ensuring that air speeds in the box were low and the pressure within the box was uniform. The plan area was large enough to accommodate at least a 4 × 4 array of tiles (Fig. 5b). The box was pressure tested to ensure there were no leaks. The tiles were laid as they would be on a roof, with rafters and battens, but no underlay or under-roof. All non-representative joints and tile junctions were sealed, except for a minimum of 4 sidelocks and 4 headlocks in the middle of the tile array (Fig. 5c). The flow rate was controlled by a variable speed fan and was measured using an EDRA6 anemometer or an orifice plate, depending on the flow rate. A digital manometer measured the difference between the pressure within the wooden plenum (Fig. 5d) and the laboratory; i.e. the pressure difference across the tiles. The flow rate was adjusted to achieve a target pressure drop over a range of set values. Additionally, the laboratory pressure and temperature were measured to calculate the local air density ($\rho$).

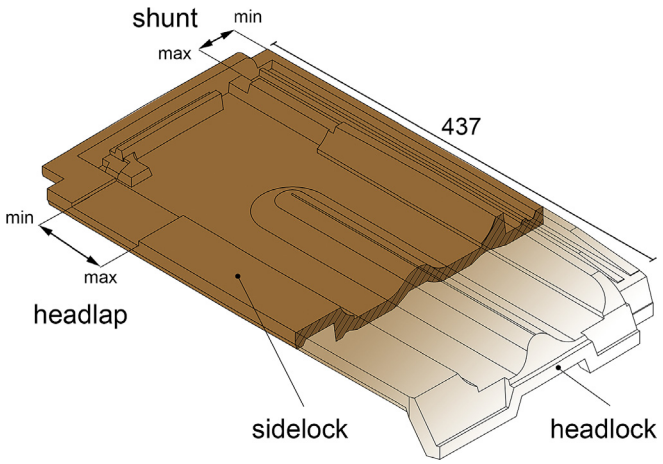


**Fig. 3.** Basic project model (PM_00).

To account for possible Reynolds number effects a series of target pressure differences were studied from 2 Pa up to 100 Pa. The lower limit was set to obtain a reasonable level of confidence in the measurements, which have an accuracy of ±0.1 Pa. The upper limit was less likely to be achieved by the more air-open tile designs. A reversible fan means this pressure difference range could be applied by blowing or sucking the air through the gaps in the tiles, to understand whether the tile geometry affected the findings.

Using Equation (1) that relates volume air flow rate (Q) to pressure difference ($\Delta P$), the aerodynamic area ($C_d \cdot A$) and flow regime radix ($n = 0.5$ for turbulent flows and $n = 1$ for laminar flows) can be found using a power law curve fit.

$$\text{Air flow rate, } Q = C_d \cdot A \cdot \sqrt[n]{\frac{2\Delta P}{\rho}} \quad (1)$$

In addition to performing the experiment with the tiles laid as normal, it was repeated using different arrangements in terms of "*shunt*" and "*headlap*" between tiles (Fig. 2), that define how much the tiles overlap at the edges. This was to investigate the effect of increased air permeability on the results and to provide extra data points for the calibration of the numerical model. "*Shunt*" refers to how much the tile on one side covers the adjacent tile (allowing adjustment of the tile spacing across the roof slope; i.e., parallel to the ridge), whereas the "*headlap*" refers to how much of the upper tile covers the lower tile (allowing adjustment of the tile spacing up the roof slope; i.e., perpendicular to the ridge). The size of the gaps between the tiles that result from their "*shunt*" and "*headlap*" positions are a function of the tile's original design and how that is affected by distortion during the manufacturing process. For example, two tiles at "*maximum shunt*" are as far away from each other as they can realistically be on a roof, but that doesn't mean that more air can go through the larger gap between them, because there may be features on the sidelock of the tiles that have come into contact and closed the air paths.

The results of the air permeability tests with the *SP* standard production (type 2050) are given in Table 1 and Fig. 8. According to the *SP* geometry, the *"headlap"* varies between a minimum of 61 mm to a maximum of 91 mm; the *"shunt"* varies in the range 33 mm–39 mm.The air flows are in the turbulent regime and $n$ approaches 0.5 as the air permeability increases. For this particular tile there is a corresponding increase in air permeability when either the *"shunt"* or *"headlap"* are increased. Also this behaviour is the same whether the air is blown or sucked through the tile array.

### 2.2. Numerical model

The finite-element code COMSOL Multiphysics V5.2 was implemented for solving the 3D, steady-state, incompressible fluid flow problem, using the RANS-based standard k-ε turbulence model. All 3D domains replicated the geometry of the rig built at the Monier Technical Centre, in terms of plenum and real tile geometries; however, to reduce the number of elements, the domain was optimised by assuming that representing the sealed tiles was unnecessary. Therefore that section was reduced to a smaller volume, only including an array of tiles, equivalent to the borders of the four tiles left unsealed on the test rig (Fig. 6). Additionally, an upper box was introduced to set the boundary conditions simulating the wind field over the tiles; its size was chosen to limit the finite element growth and the impact on the local flow field between tiles.

The *SP* – standard production model was imported from the

Please cite this article in press as: Bottarelli M, et al., CFD analysis of roof tile coverings, Energy (2017), http://dx.doi.org/10.1016/j.energy.2017.03.081

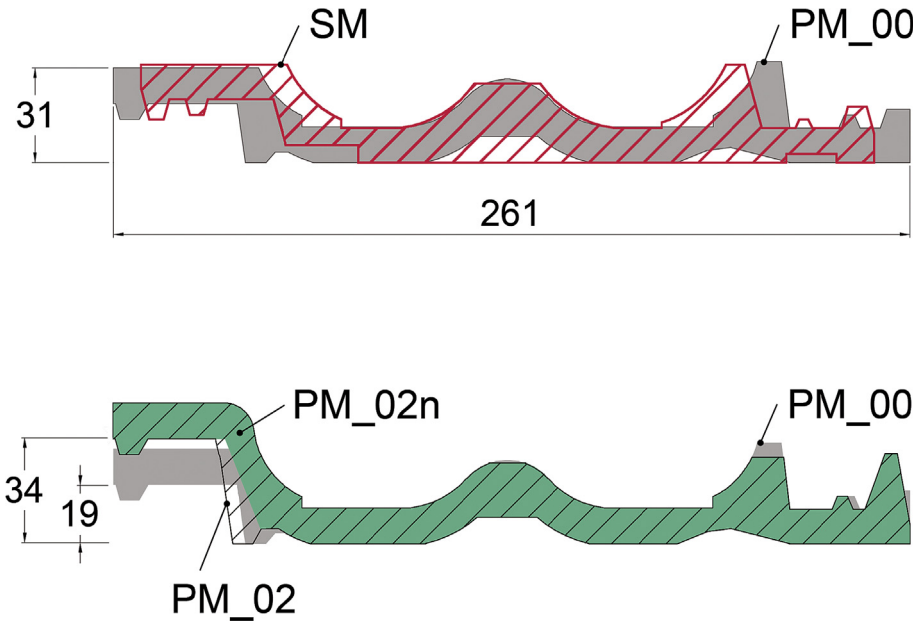


**Fig. 4.** Comparative sections between standard (SM) and basic project model (PM_00), and among basic project model (PM_00) and its two evolutions (PM_02, PM_02n).

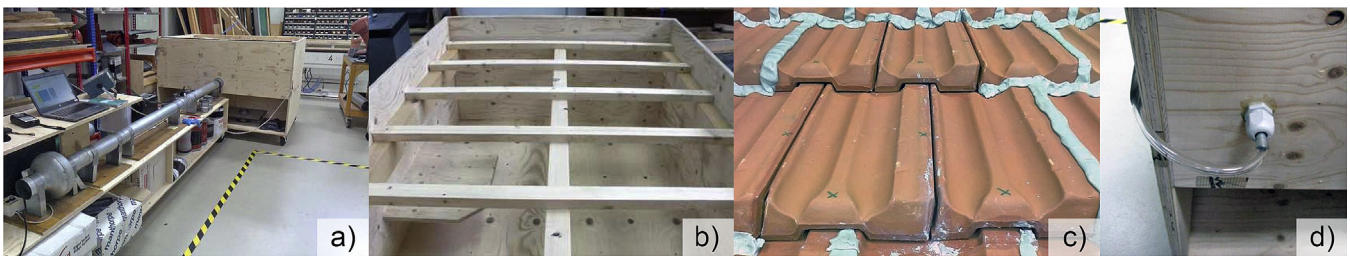


**Fig. 5.** Air permeability test rig (a), Wooden plenum chamber (b), Tile assembly of SP – standard production, type 2050 (c), Pressure reading location (d).

**Table 1**
Parameters of the experimental test (SP – standard production, type 2050).

| Parameter | Blowing | | | | Sucking | | | |
|---|---|---|---|---|---|---|---|---|
| "Shunt" | Max | Mid | Mid | Min | Max | Mid | Mid | Min |
| "Headlap" | Mid | Max | Mid | Mid | Mid | Max | Mid | Mid |
| Aerodynamic area ($C_d \cdot A$), [$mm^2$] | 2870 | 2610 | 2390 | 2000 | 3010 | 2720 | 2490 | 2160 |
| Flow regime radix (n), [–] | 0.546 | 0.541 | 0.552 | 0.550 | 0.548 | 0.547 | 0.556 | 0.555 |
| Specific aerodynamic area, [$cm^2$/tile] | 7.17 | 6.51 | 5.98 | 5.00 | 7.53 | 6.80 | 6.22 | 5.41 |

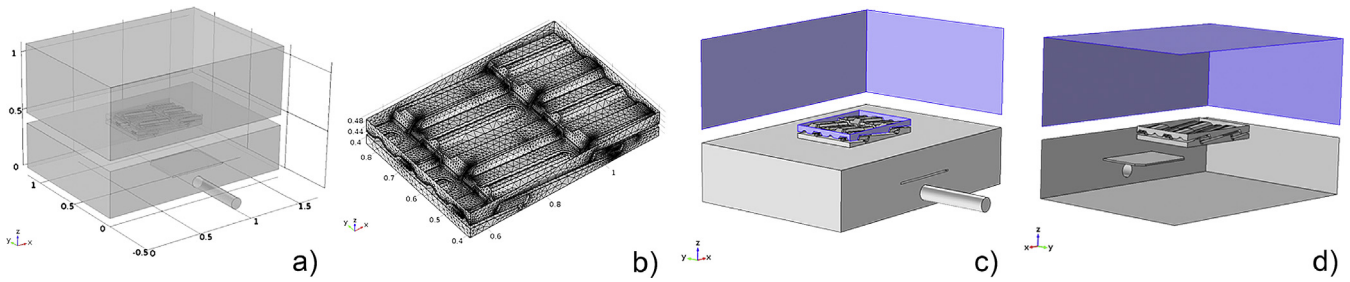


**Fig. 6.** 3D model domain (a), mesh detail (b), model sides with open boundary (c, blue) and wind boundary condition (d, blue). (For interpretation of the references to colour in this figure legend, the reader is referred to the web version of this article.)

industrial CAD, with minimal pre-processing to remove surface mesh features that can lead to problems in the CFD simulation stability and restrict control over the mesh sizing options. In order to model the distortion of individual real clay tiles (due to the drying and firing processes that can reach temperatures in excess of 1000 °C) with the regular, identical CAD geometry, the spacing

Please cite this article in press as: Bottarelli M, et al., CFD analysis of roof tile coverings, Energy (2017), http://dx.doi.org/10.1016/j.energy.2017.03.081

between the overlapping tiles was considered as a calibration parameter, as detailed in the following paragraph.

In terms of boundary conditions, a different approach was taken for the calibration method and the parametric analysis. In the calibration case, the domain with the 3D model of the *SP* – standard production was set to solve the experimental box where the air was sucked through the tiles. At the top an open boundary condition was imposed, with a relative pressure set to 0 Pa, and at the end of the pipe a series of lower pressures (−1/−2/−3/−4/−5/−10 Pa) were applied; all other surfaces were defined as no-slip walls. Similarly it was then carried out for all other models, to compare the results with *SP* model.

In the parametric case, the *SM* – standard model and the *PM_02n* – project model 02n were placed in the domain and solved with different boundary conditions to account for the modelling of different wind directions and intensities. Therefore, six sides were set as open boundary conditions (blue side in Fig. 6c), whereas the wind inlet condition was imposed on the remaining three sides (blue side in Fig. 6d). This arrangement was chosen because the wind was considered to be blowing only from one side with different directions (0°, 15°, 30°, 45°, 60°, 80°) and intensities (0.5, 1.0, 2.0, 5.0 m/s). Moreover, instead of moving the tiles to follow different angles of incidence (10°, 20°, 30°), the wind direction was configured with an corresponding incidence. As a consequence, the three components of the velocity vector were defined as follows: Equation (2): wind velocity vectors.

$$\text{wind velocity vectors}: \begin{cases} u = i\cdot\cos(\alpha)\cdot\cos(\beta) \\ v = i\cdot\cos(\alpha)\cdot\sin(\beta) \\ w = -i\cdot\sin(\alpha) \end{cases} \quad (2)$$

where $i$ defines the wind intensity (m/s), $\alpha$ is the angle of incidence (deg), $\beta$ is the wind direction (deg), and $u$, $v$, $w$ are the wind components in x, y, z direction (m/s), respectively.

To understand the reliability of the numerical results, a mesh dependency analysis was performed. Fig. 7 shows the air flow rate at the outlet pipe against the number of finite elements, when a wind of 1.0 m/s is blowing orthogonally against a 30° inclined roof. As a balance between mesh size and solution CPU time, the first and coarsest mesh was considered an acceptable compromise, according to the goals of the study and the simplifications already introduced in the domain.

## 3. Results and discussion

The calibration between experimental and numerical model was sought by varying the gap between overlapping tiles up to obtain the same relationship between pressure difference and air flow rate. Preparatory models showed that the surface roughness effects was negligible. Then, the resulting gap was applied to the novel tile shapes to evaluate the additional air permeability compared to the calibrated model. Further simulations included a parametric analysis to investigate the effect of varying local wind conditions blowing over a roof tile coverings on the air flow rates through the tiles.

### 3.1. Model calibration

The first CFD model consisted of the same tile shape tested in laboratory (type 2050, *SM* – standard model), with the aforementioned simplification of the four unsealed tiles, mid shunt and maximum headlap, and an initial gap of 0.8 mm applied uniformly between overlapping tiles. This preliminary gap corresponded to the deformation due to the firing process, that may be up to the 5–8% of the mould height, according to the manufacturer. To compare the numerical results with the experimental measurements, a point probe was used in the numerical model to monitor the pressure inside the box. The probe was located in same position as the real pressure probe.

Fig. 8 shows all four experimental test cases (*SP_*.**), combining different shunts (*mins, mids, maxs*) and headlaps (*minh, midh, maxh*). In the same figure are the results of five simulation cases varying the gap from 0.8 mm to 3.5 mm (*SM_*.**), as previously mentioned. It is evident that the slope of the numerical predictions of the standard model (*SM*) is similar to the experimental measurements (*SP*). Hence, it appears that the pressure difference is mainly related to open area and the labyrinthine path formed by the gap between tiles. As shown in Fig. 8, the results for the first case (*SM_0.8*) under-predicted the air flow rate compared with the experimental measurement selected to be the benchmark (*SP_mids_maxh*). Therefore, the gap was enlarged up to 3.5 mm (*SM_3.5*) for better agreement with experiment, and the 3.0 mm case (*SM_3.0*) was selected as the best match.

### 3.2. Air permeability of a novel tile design

The calibration parameter, which defined a 3.0 mm gap between an existing tile geometry, was used during the evaluation of the novel tile design (*PM_00*) and 10 variations of that design, not shown here for sake of brevity. That was assumed because the project model and its variants had a very similar shape to the

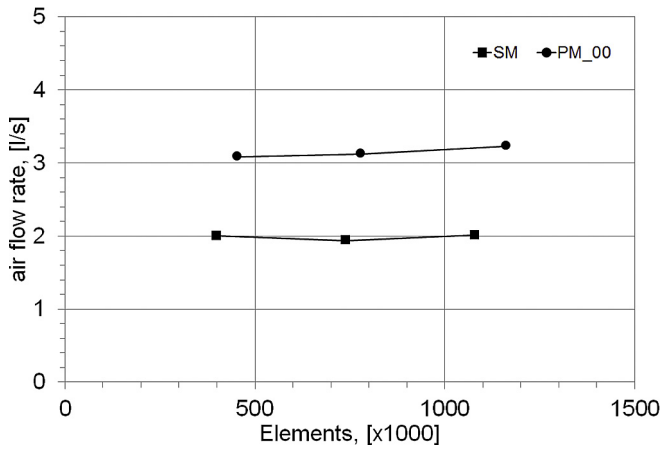


**Fig. 7.** Mesh dependency of the standard and the basic project models.

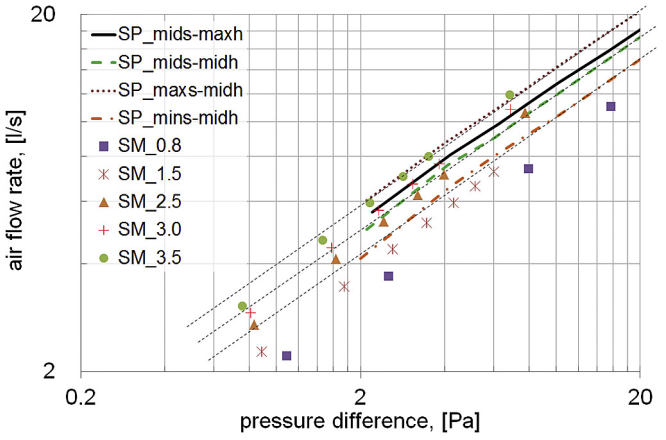


**Fig. 8.** Air permeability of the existing shape (SP – standard production, SM-standard model).

Please cite this article in press as: Bottarelli M, et al., CFD analysis of roof tile coverings, Energy (2017), http://dx.doi.org/10.1016/j.energy.2017.03.081

original design, and the small variants only included modifications – to the side, or the front, or both – with the aim of increasing the air permeability in different wind conditions.

Three representative cases are presented here: the base novel design (*PM_00*), a modification to the sidelock (*PM_02*), and an additional modification to the headlock (*PM_02n*). In Fig. 9, the numerical results of the calibrated standard model (*SM_3.0*) and the base new tile design (*PM_00*) are shown together with those of the new tile variants (*PM_02*, *PM_02n*). All results were obtained by simulating the sucking mode at the pipe but, based on the experimental results reported in Table 1, there would be no significant difference in the behaviour whether the air was flowing in to or out of the gap between the tiles. The cases *SM_3.0* and *PM_00* agree well with the experimental measurements of the existing tile (*SP_mids_maxh*), therefore confirming the validity of applying the calibration rule from the standard model to the project model (3.0 mm).

The sidelock modification in the first variant (*PM_02*) increased the air flow rate by approximately 20%, compared with the base novel tile (*PM_00*); however, improvements of this magnitude can be lost through non-uniformities in the manufacturing process. Analysing the flow path through the tiles, it was found out that the labyrinthine path formed by the gap between tiles, which required to prevent the ingress of driving rain, had a very small cross-section causing a high pressure difference. As a consequence, a new headlock pattern was designed to yield a lower pressure difference, whilst retaining the driving rain function, and this was implemented into variant *PM_02n,* as shown in Fig. 10. The enhanced geometry of the sidelock, higher and with a larger opening, allows the air to flow in the ASV when exposed to a wind blowing sideways. The performance of this variant was significantly better, increasing the air flow rate up to 100% above that of the base novel tile design (*PM_00*).

### 3.3. Parametric analysis

Although imposing fixed pressure differences across the tiles provides a useful means of comparing air permeability, in reality that pressure difference is due to the action of the wind over the whole building envelope, which generates a complex flowfield with large-scale end small-scale flow separations, reversals, etc. according to building topology and wind direction. However, the analysis of a whole building needs a full scale 3D model, that is beyond the commonly available computational resource. Instead, for the purposes of this preliminary assessment of the air permeability of roof tile coverings, it was decided to accept the limitation

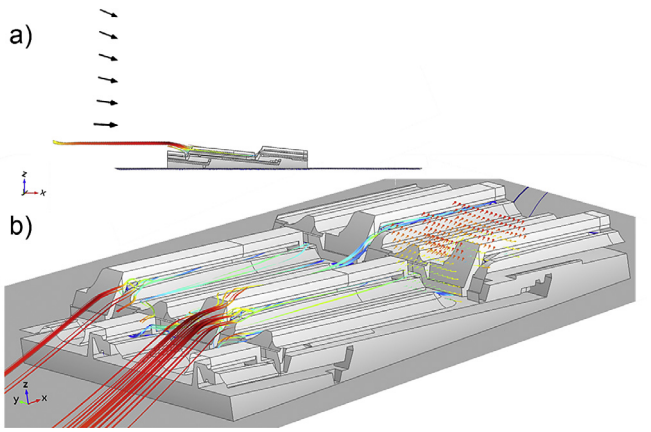


**Fig. 10.** Wind field affecting the roof (a) and streamlines through the tiles for PM_02n type (b).

of using uniform wind condition for the boundary conditions. Therefore, the standard model (*SM*) and the best-performing novel tile design variant (*PM_02n*) were parametrically analysed using a set of 72 wind conditions: four wind speeds ($i = 0.5, 1.0, 2.0, 5.0$ m/s), three angles of incidence ($\alpha = 10°, 20°, 30°$) and six horizontal wind directions ($\beta = 0°, 15°, 30°, 45°, 60°, 80°$), as indicated in Fig. 2.

In Fig. 11, the air flow rate for the *SM* and *PM_02n* cases is shown for an angle of incidence of 10° ($\alpha$), according to the wind angle ($\beta$) and the wind intensity ($i$). In Figs. 13 and 15 the equivalent results are reported for an angle of incidence of 20° and 30°, respectively. The results for the *SM* case show the expected decrease in air flow rate as the wind angle ($\beta$) moves from facing the tiles head-on around to side-on; however, the opposite is true for the *PM_02n* case and the new design always gives higher air flow rates than the standard model. This is mainly due to the sidelock modification allowing more air flow in through the side of the tile. The improvement is significant, especially at lower wind intensities; i.e., at $\beta = 45°$ wind direction and $\alpha = 20°$ the improvement is 87%, 68%, 64% and 60% at a wind velocity of 0.5, 1.0, 2.0 and 5.0 m/s, respectively.

In Fig. 12, the air flow rate for the *SM* and *PM_02n* cases is shown for an angle of incidence of 10° ($\alpha$), according the pressure difference between an internal and external point probe. The internal probe is the same one used for the comparison with the experimental rig, located in the bottom corner of the plenum; the external probe is located centrally at the top of the domain. In the figure, all

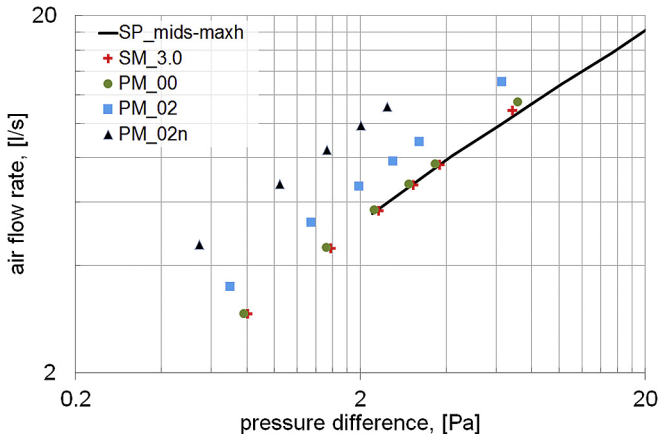


**Fig. 9.** Air permeability comparison between experimental and numerical analysis.

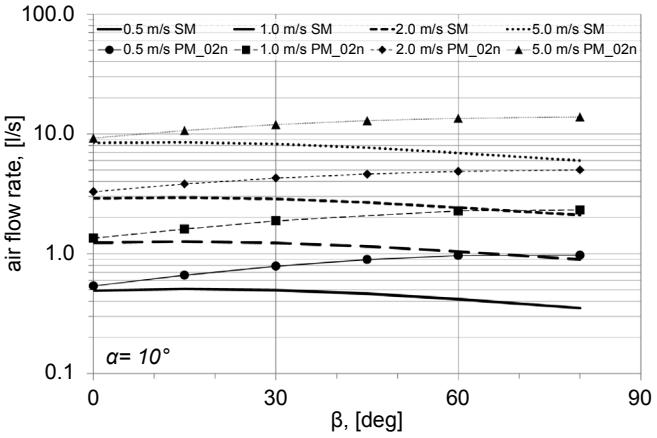


**Fig. 11.** Air permeability as a function of wind direction: angle of incidence 10°.

Please cite this article in press as: Bottarelli M, et al., CFD analysis of roof tile coverings, Energy (2017), http://dx.doi.org/10.1016/j.energy.2017.03.081

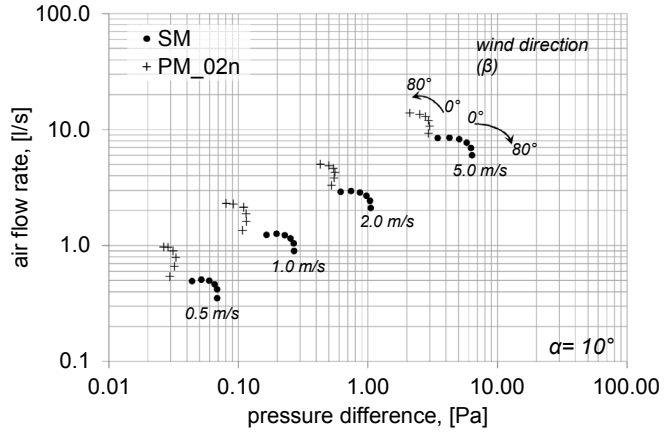


**Fig. 12.** Air permeability as a function of pressure difference: angle of incidence 10°.

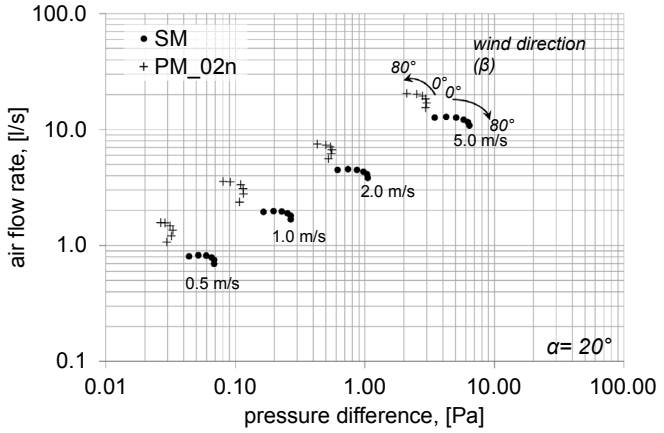


**Fig. 14.** Air permeability as a function of pressure difference: angle of incidence 20°.

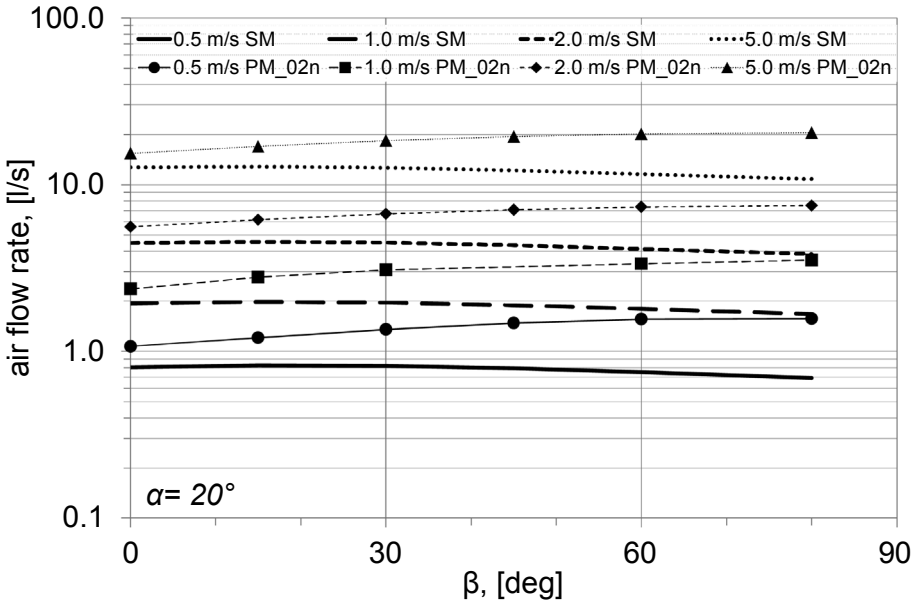


**Fig. 13.** Air permeability as a function of wind direction: angle of incidence 20°.

four cases related to different wind intensity, and six cases for the different wind direction are presented. In Figs. 14 and 16 the equivalent results are reported for an angle of incidence of 20° and 30°, respectively. Despite starting from similar values at 0° wind direction, the *SM* case and the *PM_02n* case then diverge in clockwise and anticlockwise directions, respectively, confirming the earlier observation about the increasing air flow rate with wind direction in the *PM_02n* case.

## 4. Conclusion

A combined experimental and numerical analysis of roof tile coverings was carried out to design novel Marseillaise tile shapes, towards a higher air permeability through the tile overlapping, that takes part in the above sheathing ventilation of ventilated roofs.

Preliminary tests measured the air permeability of a roof tile covering built with an existing Marseillaise tile shape, using the pressure difference across the tiles at measured air flow rates controlled by a variable speed fan. The results were used as the benchmark to calibrate a CFD model replica of the test rig, in which the 3D model of the existing tiles was implemented. The calibration was then used as the basis for analysing the air permeability

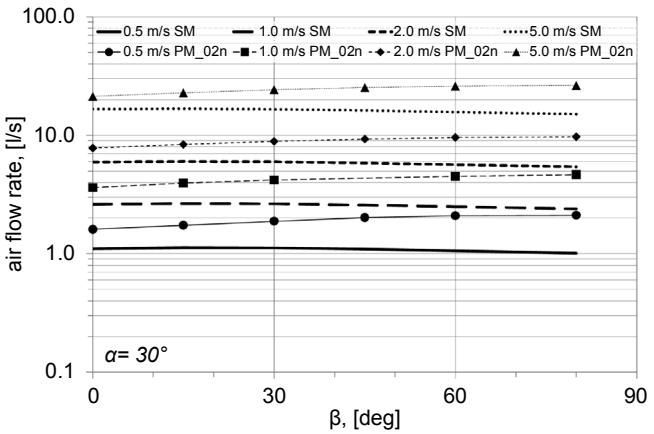


**Fig. 15.** Air permeability as a function of wind direction: angle of incidence 30°.

Please cite this article in press as: Bottarelli M, et al., CFD analysis of roof tile coverings, Energy (2017), http://dx.doi.org/10.1016/j.energy.2017.03.081

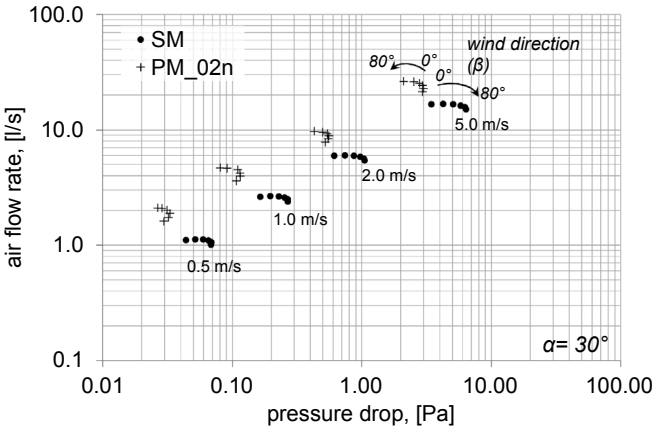


**Fig. 16.** Air permeability as a function of pressure difference: angle of incidence 30°.

performance of a novel Marseillaise type design. Following detailed air flow path analysis through the tile lock features required to prevent driving rain ingress, it was possible to design novel tile variants which gave an improvement in the air flow rate of up to 100%.

Finally, the performance of the novel shapes were numerically analysed studying the impact of the wind blowing over the roof tile coverings. Four wind speeds ($i$ = 0.5, 1.0, 2.0, 5.0 m/s) were simulated blowing over the tiles, with angles of incidence ($\alpha = 10°$, 20°, 30°) and six horizontal wind directions ($\beta = 0°$, 15°, 30°, 45°, 60°, 80°), to represent a parametric analysis of 72 wind conditions. Contrary to the reduction in air flow rate when the wind direction moves from directly up the roof tile head to coming in from the side, as seen with the existing tile shape, the modification to the sidelock in the novel design variant results in the air flow rate increasing as the wind direction changes. This effect was evident at all angles of incidence and wind speeds modelled. It is acknowledged that the real flowfield over a building is both complex and non-uniform, but it is anticipated that the improvements modelled here will have a practical effect in the physical world.

As one of the main methods of mitigating solar gain into the living space, any improvement in air permeability achieved by the novel tile shapes presented here (and the corresponding increase in convective heat transfer by the above sheathing ventilation of a ventilated pitched tiled roof) will increase the effective thermal insulation and lead to improved energy savings for space cooling in hot climates. The focus of the next stage of the LIFE HEROTILE European project will be to investigate this effect further using field measurements on mock-up and real-scale buildings, in addition to extended numerical analysis.

## Acknowledgements

This work was conducted as a part of the preliminary action A.1 of the European project titled LIFE HEROTILE - *High Energy savings in building cooling by ROof TILEs shape optimization toward a better above sheathing ventilation* (LIFE14 CCA/IT/000939, http://www.lifeherotile.eu/), co-funded by the EU LIFE programme "Climate Change Adaptation".

## References

[1] Lee S, Park SH, Yeo MS, Kim KW. An experimental study on airflow in the cavity of a ventilated roof. Build Environ 2009;44:1431–9.
[2] Dimoudi A, Androutsopoulos A, Lykoudis S. Summer performance of a ventilated roof component. Energy Build 2006;38:610–7.
[3] D'orazio M, Di Perna C, Principi P, Stazi A. Effects of roof tile permeability on the thermal performance of ventilated roofs: analysis of annual performance. Energy Build 2008;40:911–6.
[4] Madhumathi A, Radhakrishnan S, Shanthi Priya R. Sustainable roofs for warm humid climates – a case study in residential buildings in Madurai, tamilnadu, India. World App Sc J 2014;32:1167–80.
[5] Amornleetrakul O, Puangsombut W, Hirunlabh J. Field investigation of the small house with the ventilated roof tiles. Adv Mater Res 2014;931–932:1233–7.
[6] Ramos J, Almeida L, Pitarma R. Experimental study on a naturally ventilated ceramic tile roof as potentially beneficial for the thermal performance of housing, Materials and Technologies for Energy Efficiency. Boca Raton, FL, USA: Brown Walker Press; 2015.
[7] Sandberg M, Moshfegh B. Ventilated-solar roof airflow and heat transfer investigation. Renew Energy 1998;15:287–92.
[8] De With G, Cherry N, Haig J. Thermal benefits of tiled roofs with above-sheathing ventilation. Int J Build Phys 2009;33:171–94.
[9] Miller W, Keyhani M, Stovall T, Youngquist A. Natural convection heat transfer in roofs with above-sheathing ventilation, thermal performance of the exterior envelopes of buildings X. Ashrae Therm X, Clearwater Beach, FL: ASHRAE; 2007.
[10] Ciampi M, Leccese F, Tuoni F. Energy analysis of ventilated and micro-ventilated roofs. Sol Energy 2005;79:183–92.
[11] Gagliano A, Patania F, Nocera F, Ferlito A, Galesi A. Thermal performance of ventilated roofs during summer period. Energy Build 2012;49:611–8.
[12] Bianco V, Diana A, Manca O, Nardini S. Thermal behavior evaluation of ventilated roof under variable solar radiation. Int J Heat Technol 2016;34:346–50.
[13] Bottarelli M, Bortoloni M, Zannoni G. Prestazioni termiche estive di tetti ventilati a manto discontinuo. In: Conference proceedings, VII Italian Association of energy management conference. Rende: UNICAL; 2013.
[14] Bottarelli M, Zannoni G, Allen R, Cherry N. CFD analysis and experimental comparison of novel roof tile shapes. In: Abstract book, international heat transfer symposium 2016. Nottingham: UON; 2016.
[15] BS 5534. Slating and tiling for pitched roofs and vertical cladding – code of practice. BSI Standards Publication; 2014.